Innovative Ni-Al2O3 substrate including a graded interface fabricated by SPS: Application for power modules

Romain Raisson, Sophie Guillemet-Fritsch, Pascal Dufour, Aurelie Boisard, Cyrille Duchesne, Paul-Etienne Vidal

▶ **To cite this version:**

Romain Raisson, Sophie Guillemet-Fritsch, Pascal Dufour, Aurelie Boisard, Cyrille Duchesne, et al.. Innovative Ni-Al2O3 substrate including a graded interface fabricated by SPS: Application for power modules. Ceramics International, 2025, ⟨10.1016/j.ceramint.2025.07.132⟩. ⟨hal-05164963⟩

HAL Id: hal-05164963

https://hal.science/hal-05164963v1

Submitted on 16 Jul 2025

HAL is a multi-disciplinary open access archive for the deposit and dissemination of scientific research documents, whether they are published or not. The documents may come from teaching and research institutions in France or abroad, or from public or private research centers.

L'archive ouverte pluridisciplinaire **HAL**, est destinée au dépôt et à la diffusion de documents scientifiques de niveau recherche, publiés ou non, émanant des établissements d'enseignement et de recherche français ou étrangers, des laboratoires publics ou privés.

HAL Authorization

Innovative Ni-Al_2O_3 substrate including a graded interface fabricated by SPS: Application for Power modules

R. RAISSON[(a)], S. GUILLEMET-FRITSCH[(b)], P. DUFOUR[(b)], A. BOISARD[(c)], C. DUCHESNE[(d)] and P. VIDAL[(e)]

[(a)]*E2S-UPPA, Avenue de l'Université 64012 Pau*

[(b)]*CIRIMAT, INP CNRS, Université Toulouse , 118 Route de Narbonne, 31062 Toulouse*

[(c)]*SAFRAN TECH, Rue des jeunes Bois, 78117 Châteaufort*

[(d)]*DEEP CONCEPT, 2 Av. du Président Pierre Angot, 64000 Pau*

[(e)]*LGP, INPT-ENIT, Toulouse University - UFTMiP, 47 avenue d'Azereix, 65016 Tarbes*

Abstract

To enhance the efficiency of power modules, the development of new substrate technologies is essential. This article describes the design of a nickel-alumina substrate produced through co-sintering via spark plasma sintering (SPS), utilizing a sacrificial alumina layer approach. An Ni-Al_2O_3 substrate is achieved after sintering at 1150°C under a pressure of 50 MPa. The substrate has two thick nickel metal layers, making it suitable for applications with high current densities. A well-defined interface, of thickness 30–40 µm, is formed. It consists solely of pure nickel and pure alumina with no secondary phases. The mechanism behind the formation of this interface is attributed to thermomechanical deformation during the sintering process. Mechanical tests, including shear and pull tests, demonstrate adhesion strength that meets aeronautical standards. This one-step approach, which saves both energy and time, can be applied across various fields utilizing technical ceramics.

Keywords

SPS ; Graded interface ; Substrate ; Ni-Al_2O_3

1 Introduction

The demand for reliable and efficient power electronics devices drives continuous efforts to develop increasingly compact solutions, particularly in sectors such as rail transport and aeronautics [1]. More generally, the power-to-weight ratio of devices is critical in transport applications. For high-power applications, converters made of multiple power modules are employed. This study focuses on these modules, aiming to design devices capable of supporting

high voltages (>1kV), high currents (>100 A) thanks to parallelized semi-conductors' devices, and elevated operating temperatures (>150°C) [2]. The increase in temperature is primarily due to the advances in semiconductor chip technology. In recent years, silicon chips have been replaced by silicon carbide chips (MOSFET SiC). The heating of these chips induces local temperature variations, leading to thermomechanical stresses in the surrounding environment and the failure of the device. These stresses guide the design of modules toward the use of metallized ceramic substrates, which serve as mechanical support, current collectors, thermal interface and obviously, dielectric insulation. The metallized substrate's reliability is crucial for the proper functioning of the module [3,4].

Several metallized substrate technologies have emerged in recent decades. These include ceramic substrates such as silicon nitride (Si_3N_4), aluminum nitride (AlN), and alumina (Al_2O_3)[5–7]. The three ceramics are listed in reverse order of cost. Each material offers different properties' advantages: for instance, silicon nitride provides excellent flexural strength, aluminum nitride has the highest thermal conductivity. Alumina stands out for its high thermal expansion coefficient (CTE) of 6,8-9 10^{-6}/°C, which matches more closely with those of metals (8 10^{-6}/°C to 25 10^{-6}/°C). Lower CTE difference reduces interfacial stress during thermal variations and enhances the substrate's durability [8]. Known reliability results establish the superiority of Si_3N_4 to face severe thermal stress because of its mechanical properties, despite its higher cost [5], whereas alumina is the worst. The choice of substrate depends on the thermal environment, the cost of assembly and the desired durability. Nickel has a lower coefficient of expansion than copper, which reduces thermal expansion problems. With this metallization, one can imagine using alumina as a ceramic by working on the interface and improving the reliability of the substrate. In this context, the present work focuses on developing alumina metalized substrates using a new approach.

Various methods exist for metallizing ceramic substrates [6,9–16]. Direct Bonding [17,18] are distinguished of Active Metal Brazing (AMB) [13,14]. Direct Bond Copper (DBC) [6,12] involves sintering copper onto the alumina or aluminum nitride, forming a copper oxide bond at

the interface. Direct Aluminum Bonding (DAB) [15,16] consist of deposition of an aluminum layer on alumina due to aluminum's natural affinity for aluminum oxide. However, this method leads to more complex package's assembly processes, as dice brazing is an issue on aluminum. AMB uses a metal alloy, typically silver-based, which reacts with the ceramic, typically silicon nitride. All these methods require an initial ceramic shaping step, followed by metallization.

The co-sintering of materials offers a way to produce multi-material objects in a single step [19–21], while reducing the process time. With the co-sintering there is no need to etch the ceramic substrate. The main challenge to overcome deals with the difference in sintering temperatures and thermal expansion coefficients between the ceramic and metallic materials [22]. The level of residual stresses is directly proportional to the difference in thermal expansion coefficients and the sintering temperature [23]. To minimize the development of these stresses, it is essential to select the lowest possible sintering temperature and materials with closely matched thermal expansion coefficients [23]. Also the thickness of the materials plays an important role in obtaining crack-free assemblies [24].

The objective of this study is to assess the feasibility of a one-step Nikel-ceramic assembly process that can be directly employed for the fixation of power electronic components, while meeting the stringent requirements of aerospace standards.

In this study, the single step fabrication of an alumina-nickel substrate using SPS sintering is described. A sacrificial material approach to limit the thickness of the metallic layer [24] is developed. The substrates are produced in multiple samples, and semiconductor chips are soldered onto their surface. Mechanical tests are conducted to highlight their potential use in aeronautic applications.

In the first part, the characteristics of the starting materials used to fabricate the device, with a particular focus on the sintering treatment, are presented. In the second part, we provide structural and microstructural characterizations of both the substrate and the interface. Thirdly,

the studies on mechanical resistance, including tests on bonding wires and shear tests for chip detachment, are detailed. Finally, we draw conclusions based on the results obtained.

2 Materials and Methods

2.1 Materials preparation and sintering

The substrate was prepared using Al_2O_3 nanopowder (d50 = 0.12µm, ≥98% purity) sourced from Baikowski (BMA15) [25] and an annealed nickel foils with a thickness of 127 µm (≥99% purity), purchased from VWR [26]. The substrate sintering is carried out in graphite molds with an internal diameter of 10 millimeters and a depth of 30mm (ISO 68, Toyo Tanzo) at the French National Flash Sintering Platform (PNF^2). The mold is lined with a graphite foil, and the quantity of Al_2O_3 powder to be introduced is calculated in order to obtain a final thickness of 2 mm. A layer of alumina is deposited at the bottom of the mold and compacted using a manual press. The targeted thickness of this layer is 100µm after sintering. Next, a pre-flattened nickel foil with a diameter of 8 mm is placed at the center of the mold, on top of the alumina powder, without applying pressure at this stage. Additional alumina powder is then introduced into the mold to achieve a total thickness of 2 mm after sintering. A second 8-mm nickel foil is positioned in the center of the mold. The entire assembly is compacted to ensure uniform distribution of the powder around the nickel foil. A final layer of alumina (100µm after sintering) is added before the mold undergoes final compaction. These upper and lower layers of alumina ensure that the nickel is mainly heated by the die and not by Joule effect. As described in references [27,28], SPS induces a difference of behavior between metal and ceramic due to the electric field impact. The Fig. 1 shows the mold after sintering with targeted dimension of the layers (a) and a picture of the final substrate after polishing (b). The temperature measurement is conducted in a designated hole located at the center of the mold, in close proximity to the sample.

Sintering was performed by Spark Plasma Sintering (SPS) apparatus (FUJI 632Lx from Fuji Electronic Industrial CO., Japan) using pulsed DC sources. Firstly, a pre-compaction step (50 MPa) of one minute at room temperature is performed. Secondly, the samples were sintered

under vacuum with a residual pressure of 20 Pa. The sintering cycle used is shown in the Fig. 2. The temperature is measured using a pyrometer, which begins detecting above 574°C. During the heating phase (3 minutes), a load of 3,8 MPa is applied to the mold, and the temperature reaches 600°C. Indeed, the pyrometer starts measuring. The temperature is stabilized for 3 minutes, followed by a heating ramp of 100°C/min until 1150°C is reached. At 1000°C, a load of 50 MPa is applied. The temperature and pressure are maintained for 5 minutes, after which the pressure is released (3,8 MPa) while maintaining the temperature. Finally, the cooling is performed at a rate of 12.5°C/min.

After the sintering cycle, the substrate looks like a complete alumina disc and can be easily removed from the mold. A significant adhesion occurs between the sacrificial alumina layer and the nickel. So, the two 100 µm alumina layers are removed by polishing with diamond disc to obtain a pure Ni layer on both faces. Pictures of the polishing stage are described in Fig. 3. After sintering, the nickel layer beneath the alumina can be seen (Fig. 3 (a)) by transparency. During polishing, the sacrificial layer is progressively removed (Fig. 3 (b)). The final polished sample presents a fully available Ni surface (Fig. 3 (c)). After polishing the metal/ceramic disc is named substrate and is ready for power module assembly.

2.2 Material characterization

The relative density of the samples was determined using the Archimedes principle. The morphology of the powder, the compositional mapping of the discs, and the system's integrity were examined using a scanning electron microscope (SEM) (TESCAN Vega 3) equipped with an Oxford INCA Energy Dispersive Spectroscopy (EDS) detector at an acceleration voltage of 20 kV. Structural analysis of the discs through X-ray diffraction (XRD) was conducted using a Bruker D4 Endeavor diffractometer at room temperature, with Cu Kα1 and Kα2 radiation over a 2θ angle range of 20° to 60°. A JEOL cross-section polisher (IB-19510CP) with a focused argon ion beam (FIB) was employed to section the substrate, and a SEM-FEG (FEI HELIOS 600i) microscope coupled with Energy Dispersive Spectroscopy (EDS) was used to observe the internal microstructure and the chemical composition of the substrate. For the EDS line scan the step size

is 0,9µm with a acceleration voltage of 10kV. A nanometric slide was extracted using FIB in the interface zone of a polished sample. The microstructure and chemical composition of the interface area were also analyzed by Transmission Electron Microscopy TEM (JEM-2100F) at 200 kV. EDS analysis was carried out with STEM mode at an accelerating voltage of 10 kV on the sample. In accordance with the MIL-STD-883H standard, shear tests were performed using a Royce 650 instrument equipped with an SMS-200K (210 kgf) module on SiC diode chips (0.4 × 0.4 cm) soldered onto the upper nickel metallization layer of the substrate (Fig. 4). The lower nickel metallization was soldered onto a copper support with a nickel finish. The solder used was SAC305 paste (Sn 96.5%, Ag 3%, Cu 0.5%).

3 Results and discussion

3.1 Structural and microstructural characterizations

3.1.1 Alumina

The Fig. 5 shows micrographs of the alumina powder and a fracture of the sintered alumina disc obtained after sintering at 1150 °C. The alumina powder particles are pseudo-spherical. The ceramic exhibits well-defined Grains with no significant intergranular porosity. The densification, determined from an average of five samples, reaches 99.6±0.1%.

3.1.2 Ni/Al_2O_3 substrate

Fig. 6 shows XRD analysis of the ceramic/metal interface, after the sacrificial layer has been almost completely withdrawn by polishing (Fig. 3(b)). For comparison, the XRD patterns of an alumina disc and a pure nickel foil are added. Only alpha alumina and metallic nickel are present, with no additional phase. The formation of a mixed spinel ($NiAl_2O_4$) at the interface between alumina and nickel has been reported in literature [21], for sintering treatment performed in air at temperatures above 1300°C. Here, a lower sintering temperature and vacuum atmosphere avoid the formation of the spinel phase at the ceramic/metal interface.

Further SEM observations were performed to analyze the interface. The Fig. 7 presents the micrographs of the alumina-nickel interface in the co-sintered substrate, after sectioning and

polishing. In Fig. 7 (a and d), the central nickel layer is visible, with the main alumina layer (2 mm), and the sacrificial alumina layer (100 μm). The dark zone in the nickel layer is SiC residues from polishing. A difference in density can be observed between the sacrificial and the main alumina, with the main alumina exhibiting a lower density. At the interface between the alumina and nickel, an area with intermediate contrast (Fig. 7 c and e), of thickness of 30-50 μm is observed, which is absent between the nickel and the sacrificial alumina (Fig. 7 b and f). This indicates a difference in behavior at the interface between the nickel and the bulk alumina compared to the interface between the nickel and the sacrificial alumina. Further investigations were therefore conducted on the interface formed between the alumina and nickel to understand the mechanism of formation of the interface microstructure.

The Fig. 8 presents a FEG-SEM image of the interface region between nickel and the main alumina after ion polishing. A mixed zone is observed with a thickness ranging between 30 and 40 μm. Additional Energy Dispersive Spectroscopy (EDS) analysis was performed on various areas (b, c, and d). As expected, the upper region consists of pure nickel with a slight detection of aluminum, while the intermediate zone contains nickel, oxygen, and aluminum. The lower region is composed only of oxygen and aluminum.

An average of three EDS linescan across the interface reveals a gradual variation in composition on either side of the interface. As shown in the Fig. 9, the nickel content increases from the pure alumina (aluminium + oxygen) region and reaches almost 100% of Nickel as it transitions into the nickel layer, with the alumina content decreasing inversely. A compositional gradient has thus formed at the interface, similar to the one observed for continious Functionally Graded Material (FGM) [29].

A more detailed analysis using TEM was conducted and the image obtained at the interface region (Fig. 10). The image reveals two distinctly contrasted regions (a). Energy-dispersive X-ray spectroscopy (EDS) of this area indicates the presence of nickel (b), as well as oxygen and aluminum (c and d). The spatial overlap of aluminum and oxygen suggests regions containing

alumina, whereas nickel is detected separately, implying the existence of distinct zones composed of either alumina or pure nickel. No chemical diffusion between the alumina and nickel is observed at this scale.

To further validate this observation, electron diffraction was performed on two adjacent areas at the interface of two different grains (Fig. 11). The two diffraction patterns, obtained using the same aperture, display distinctly different patterns on either side of the interface. By analyzing the distances between the diffraction spots in the reciprocal space, we identified the interplanar spacings of the target materials. The diffraction pattern (c) shows characteristic interplanar distances for the (104), (012), and (110) planes of alpha-alumina, while pattern (d) reveals the interplanar distances of the (111) and (200) planes of face-centered cubic nickel.

Hence the interface between the nickel and alumina consists of both materials, with no formation of a spinel phase. The hypothesis for the formation of this interface is illustrated in the Fig. 12. Prior to sintering, a solid nickel material is placed in contact with porous alumina powder. During the temperature rise, the nickel is compressed into the alumina on both sides. Due to its lower melting point, nickel tends to migrate into the pores of the alumina under the applied pressure during sintering. This phenomenon is enhanced as the system approaches the melting point of nickel (1453°C), making it more mobile and capable of undergoing plastic deformation (creep). The mechanism here is close to metal liquid infiltration process, which is generally processed at temperature higher than the melting point of the metal [30]. In the literature, Copper infiltration has been conducted in the SPS and the benefit of the pressure has been demonstrated [31].There is a competition between Ni infiltration and Alumina densification. The hypothesis proposed to explain the morphological differences between the main alumina and the sacrificial alumina is based on Joule heating. The Joule effect occurs only in the mold surrounding the sample. Since alumina is electrical insulator, heat diffusion takes place from the edges of the sample toward its center. It is assumed that the sacrificial alumina begins densifying earlier than the main alumina, leading faster to the elimination of its porosity and thereby limiting the formation of a graded interface.

To confirm the infiltration hypothesis, shrinkage during sintering was compared between the Ni/Al_2O_3 substrate, alumina alone and nickel alone. The aim was to achieve a final thickness of 2 mm for all discs. A micrometric nickel powder, already used in previous work [32], was chosen for this experiment to characterize the Ni foil behavior even if this is not exactly the same starting material. All samples were sintered with a sacrificial alumina layer deposited on their top and bottom without graphite foil between the powder layers. The Fig. 13illustrates the variation of shrinkage of the various samples as a function of temperature and during the dwell at 1150°C. The shrinkage of the graphite tool is deleted. It is notable that nickel shows significant shrinkage as low as 700°C, mainly due to densification occurring before the pyrometer detects a temperature higher than 574°C. Shrinkage continues to increase up to 925°C, followed by a brief stabilization during 50°C. After this stabilization phase, shrinkage resumes under load and continues to increase until the final temperature. As shown in the picture of Fig. 13, some of the nickel has creeped beyond the sacrificial alumina on the side of the punch. This behavior is therefore characteristic of nickel creep. In contrast, the shrinkage behavior of the substrate and pure alumina shows progressive densification of the alumina. During the co-sintering of the Ni/Al_2O_3 substrate (as shown in Fig. 12), under these conditions, nickel grains flows into the porosity of the thick, non-densified alumina layer due to pressure and temperature. As the temperature increases and reaches 1150°C, the alumina densifies, effectively preventing further nickel flow. This process strongly suggests a thermomechanical deformation of the nickel, thereby enhancing the adhesion between Ni and Al_2O_3. This phenomenon leads to a graded interface in the Ni/Al_2O_3 substrate. Now that the morphology and behavior of the interface have been characterized, it is necessary to subject it to mechanical testing to determine if this substrate is suitable for use in a power module.

3.2 Mechanical characterizations

The mounting of components (chips) or connectors onto the metallized substrate is a crucial step in the elaboration process of a power module. Specific aerospace standards for pull-off strength exist, based on the contact area between the components and the metallization. With six

substrates sintered and soldered under identical conditions, the average chip shear strength was 3.5 ± 0.3 kg/10^{-4} in², exceeding the standard (MIL-STD-883H) of 0.08 kg/10^{-4} in². The failure mechanism is attributed either to fracture within the solder layer beneath the chip or to cracking of the chip itself, with no evidence of delamination detected. Substrate detachment from the copper pad occurred in three out of six samples, with an average value of 19.1 ± 1.3 kg, surpassing the standard of 5 kg. The remaining three samples did not detach, even at the device's maximum capacity (200 kg.f).

In a separate test, ten 300 µm aluminum bonding wires were attached to another substrate and subjected to mechanical traction. The average pull strength was 473 ± 144 gf, well above the aerospace standard threshold of 150 gf. The results show that mastering the quality of the metal-ceramic interface, alumina can be used as a substrate for aeronautical applications.

4 Conclusion

The manuscript describes the design of a Ni-AL_2O_3 substrate with two parallel nickel metal layers within the matrix for possible applications in power electronics devices. A well-defined interface 30-40 µm in thickness is formed. Mechanical tests, including shear and pull tests, demonstrate that the adhesion between the metal and ceramic meets aeronautic standards. Building on these initial results, future work will involve a systematic investigation of thermal cycling effects, dielectric breakdown strength, and thermal conductivity of the substrates, in order to rigorously assess their suitability for power electronics applications. Preliminary measurements indicate a thermal conductivity of 26 $W \cdot m^{-1} \cdot K^{-1}$ and a dielectric breakdown strength exceeding 12.5 $kV \cdot mm^{-1}$, which meets the requirements of the intended application.

5 Acknowledgments

This work is supported by the funding PIA-ANR-16-IDEX-0002, project Energy And Solution for Environment - E2S UPPA within the framework of the EFFICIENCE Chaire. The

authors are grateful to A. Descamps for the TEM analysis and C. Josse for the SEM images after cross polishing.

6 References

[1] E. Santi, S. Eskandari, B. Tian, K. Peng, "6 - Power Electronic Modules"*Butterworth-Heinemann*, 2018: pp. 157–173. https://doi.org/10.1016/B978-0-12-811407-0.00006-4.

[2] A. Matallana, E. Ibarra, I. López, J. Andreu, J.I. Garate, X. Jordà, J. Rebollo, "Power module electronics in HEV/EV applications: New trends in wide-bandgap semiconductor technologies and design aspects," *Renewable and Sustainable Energy Reviews*. 113 (2019) 109264. https://doi.org/10.1016/j.rser.2019.109264.

[3] A. Zéanh, O. Dalverny, M. Karama, E. Woirgard, S. Azzopardi, A. Bouzourene, J. Casutt, M. Mermet-Guyennet, "Reliability of the connections used in IGBT modules, in aeronautical environment," *Int. J. Simul. Multidisci. Des. Optim.* 2 (2008) 123–133. https://doi.org/10.1051/smdo:2008017.

[4] M. Ciappa, "Selected failure mechanisms of modern power modules," *Microelectronics Reliability*. 42 (2002) 653–667. https://doi.org/10.1016/S0026-2714(02)00042-2.

[5] N. Chasserio, S. Guillemet-Fritsch, T. Lebey, S. Dagdag, "Ceramic Substrates for High-temperature Electronic Integration," *Journal of Elec Materi*. 38 (2009) 164–174. https://doi.org/10.1007/s11664-008-0571-8.

[6] F. Miyashiro, N. Iwase, A. Tsuge, F. Ueno, M. Nakahashi, T. Takahashi, "High thermal conductivity aluminum nitride ceramic substrates and packages," *IEEE Trans. Comp., Hybrids, Manufact. Technol.* 13 (1990) 313–319. https://doi.org/10.1109/33.56163.

[7] L. Roske, Th. Lebey, Z. Valdez-Nava, "High temperature behavior of ceramic substrates for power electronics applications"*IEEE*, *Chenzhen, China*, 2013: pp. 595–598. https://doi.org/10.1109/CEIDP.2013.6748139.

[8] U. M.b, A.-F. M.n, A.M. Noor, S. Rajoo, U. M.b, A.-F. M.n, A.M. Noor, S. Rajoo, "Current Issues and Problems in the Joining of Ceramic to Metal"*IntechOpen*, 2016. https://doi.org/10.5772/64524.

[9] J. Intrater, "Review of Some Processes for Ceramic-to-Metal Joining," *Materials and Manufacturing Processes*. 8 (1993) 353–373. https://doi.org/10.1080/10426919308934839.

[10] R. Asthana, M. Singh, "11 - Active metal brazing of advanced ceramic composites to metallic systems"*Woodhead Publishing*, 2013: pp. 323–360. https://doi.org/10.1533/9780857096500.2.323.

[11] T.H. Chuang, M.S. Yeh, Y.H. Chai, "Brazing of zirconia with AgCuTi and SnAgTi active filler metals," *Metall and Mat Trans A*. 31 (2000) 1591–1597. https://doi.org/10.1007/s11661-000-0169-0.

[12] J. Schulz-Harder, K. Exel, "Recent developments of direct bonded copper (DBC) substrates for power modules"2003: pp. 491–496. https://doi.org/10.1109/EPTC.2003.1298787.

[13] S. Mishra, A. Sharma, D.H. Jung, J.P. Jung, "Recent Advances in Active Metal Brazing of Ceramics and Process," *Met. Mater. Int.* 26 (2020) 1087–1098. https://doi.org/10.1007/s12540-019-00536-4.

[14] J. Shin, A. Sharma, D. Jung, J.P. Jung, "Effect of Sn Content on Filler and Bonding Characteristics of Active Metal Brazed Cu/Al2O3 Joint," *Korean Journal of Metals and Materials*. 56 (2018) 366–374.

[15] L. Dupont, “Contribution à l’étude de la durée de vie des assemblages de puissance dans des environnements haute température et avec des cycles thermiques de grande amplitude,” phdthesis, *École normale supérieure de Cachan - ENS Cachan*, 2006. https://theses.hal.science/tel-00091782 (accessed June 5, 2023).

[16] A. Lindemann, G. Strauch, “Properties of Direct Aluminum Bonded Substrates for Power Semiconductor Components,” *IEEE Transactions on Power Electronics*. 22 (2007) 384–391. https://doi.org/10.1109/TPEL.2006.889898.

[17] J.F. Burgess, C.A. Neugebauer, G. Flanagan, R.E. Moore, “The Direct Bonding of Metals to Ceramics and Application in Electronics,” *Active and Passive Electronic Components*. 2 (1976) 428415. https://doi.org/10.1155/APEC.2.233.

[18] J.F. Burgess, C.A. Neugebauer, G. Flanagan, “The Direct Bonding of Metals to Ceramics by the Gas-Metal Eutectic Method,” *J. Electrochem. Soc.* 122 (1975) 688. https://doi.org/10.1149/1.2134293.

[19] G. Antou, A. Heux, N. Pradeilles, N. Delhote, A. Maître, “Co-sintering of a ceramic-metal bilayer: Coupled experimental, analytical and numerical approaches,” *Ceramics International*. 50 (2024) 46196–46210. https://doi.org/10.1016/j.ceramint.2024.08.462.

[20] M. Imran, L. Deillon, I. Sizova, B. Neirinck, M. Bambach, “Process optimization and study of the co-sintering behaviour of Cu-Ni multi-material 3D structures fabricated by spark plasma sintering (SPS),” *Materials & Design*. 223 (2022) 111210. https://doi.org/10.1016/j.matdes.2022.111210.

[21] M. Zhang, Y. Zeng, H. Yang, X. Sun, “Interface control and mechanical properties of Al2O3–Ni laminated composites that were prepared through gel casting and hot pressing,” *J Mater Sci*. 57 (2022) 11684–11697. https://doi.org/10.1007/s10853-022-07326-1.

[22] J.A. Fernie, R.A.L. Drew, K.M. Knowles, “Joining of engineering ceramics,” *International Materials Reviews*. 54 (2009) 283–331. https://doi.org/10.1179/174328009X461078.

[23] O.M. Akselsen, “Diffusion bonding of ceramics,” *J Mater Sci*. 27 (1992) 569–579. https://doi.org/10.1007/BF02403862.

[24] K.H. Zuo, D.L. Jiang, Q.L. Lin, “Mechanical properties of Al2O3/Ni laminated composites,” *Materials Letters*. 60 (2006) 1265–1268. https://doi.org/10.1016/j.matlet.2005.11.010.

[25] “BMA15 - 4N α alumina nanosized milled powder - Baikowski®,” (n.d.). https://www.baikowski.com/en/serie/bma/ (accessed January 22, 2025).

[26] “Nickel ≥99% (metals basis), foil, annealed, Thickness: 0.127 mm,” *VWR*. (n.d.). https://fr.vwr.com/store/product/2338168/nickel-99-base-metaux-en-feuilles-recuit-epaisseur-0-127-mm (accessed January 22, 2025).

[27] L. Minier, S. Le Gallet, Yu. Grin, F. Bernard, “A comparative study of nickel and alumina sintering using spark plasma sintering (SPS),” *Materials Chemistry and Physics*. 134 (2012) 243–253. https://doi.org/10.1016/j.matchemphys.2012.02.059.

[28] C. Manière, A. Pavia, L. Durand, G. Chevallier, K. Afanga, C. Estournès, “Finite-element modeling of the electro-thermal contacts in the spark plasma sintering process,” *Journal of the European Ceramic Society*. 36 (2016) 741–748. https://doi.org/10.1016/j.jeurceramsoc.2015.10.033.

[29] J. Zygmuntowicz, P. Wiecińska, A. Miazga, K. Konopka, W. Kaszuwara, “Al2O3/Ni functionally graded materials (FGM) obtained by centrifugal-slip casting method,” *J Therm Anal Calorim*. 130 (2017) 123–130. https://doi.org/10.1007/s10973-017-6232-5.

[30] J.M. Molina, E. Piñero, J. Narciso, C. García-Cordovilla, E. Louis, “Liquid metal infiltration into ceramic particle preforms with bimodal size distributions,” *Current Opinion in Solid State and Materials Science*. 9 (2005) 202–210. https://doi.org/10.1016/j.cossms.2006.02.005.

[31] Y. Shi, W. Chen, L. Dong, H. Li, Y. Fu, “Enhancing copper infiltration into alumina using spark plasma sintering to achieve high performance Al2O3/Cu composites,” *Ceramics International*. 44 (2018) 57–64. https://doi.org/10.1016/j.ceramint.2017.09.062.

[32] R. Raisson, S. Guillemet-Fritsch, P. Dufour, P.-E. Vidal, G. Chevallier, D. Martineau, C. Duchesne, “Single step processing of an integrated FGM BaTiO3-Ni capacitor for power modules’ assembly,” *IEEE Transactions on Dielectrics and Electrical Insulation*. (2024) 1–1. https://doi.org/10.1109/TDEI.2024.3486677.

7 Figure captions

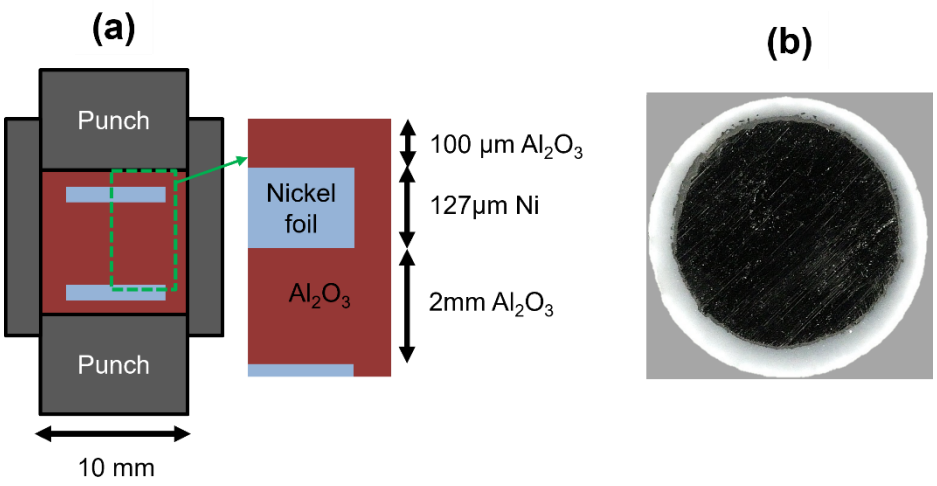

Fig. 1 Schematization of the SPS mold of the alumina-nickel substrate with the different compositions and targeted dimensions of the layers (a) and a picture of the final substrate (b)

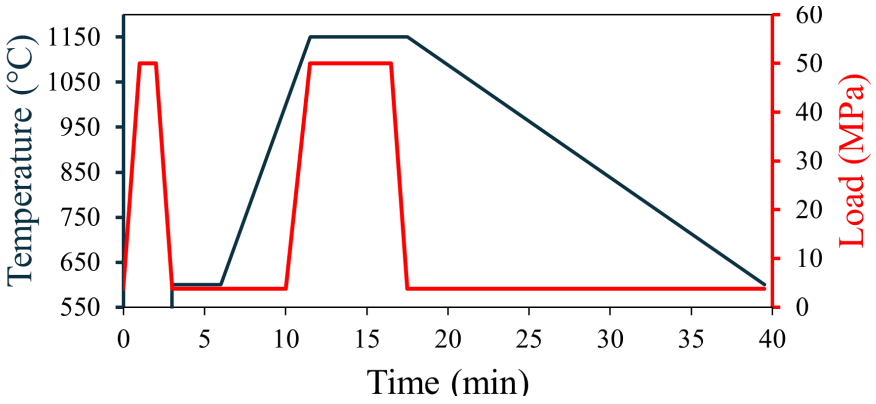

Fig. 2 Sintering cycle of the alumina-nickel substrate with the temperature variation and applied load as a function of time.

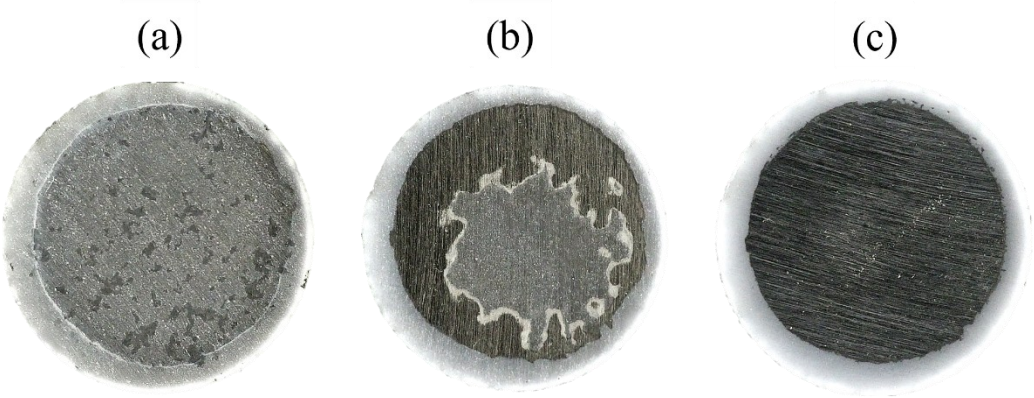

Fig. 3 Images of the substrate during polishing stage, with alumina layer on the top (a), with some of the nickel apparent but with sacrificial alumina (b) and without sacrificial alumina (c)

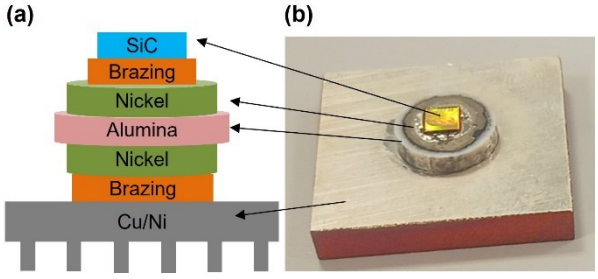

Fig. 4 Schematic representation (a) and picture (b) of the assembly

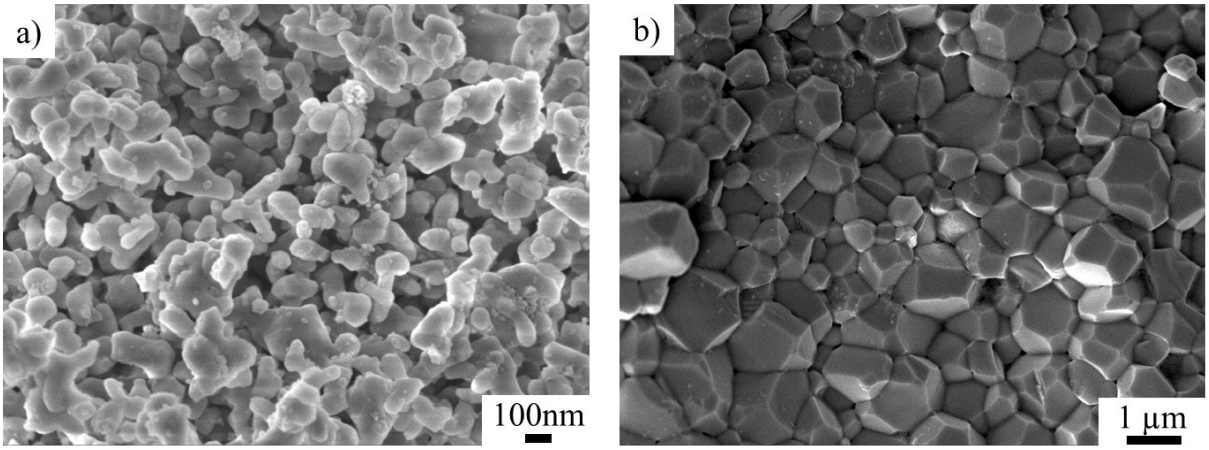

Fig. 5 SEM images of the alumina powder (a) and of an alumina fracture after sintering at 1150°C (b)

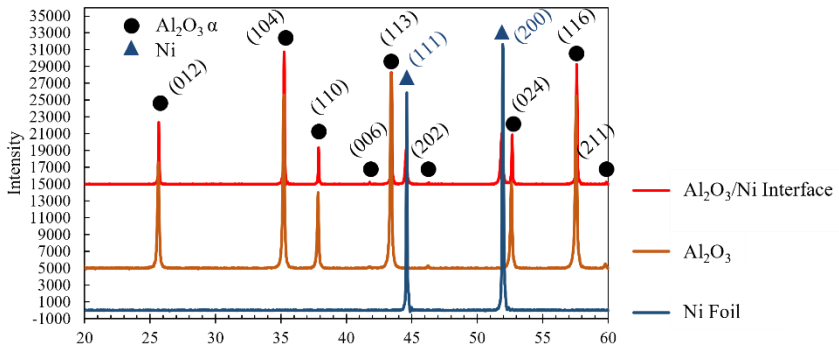

Fig. 6 XRD diagram of Ni foil, sintered alumina disc and Al_2O_3/Ni interface of the substrate after polishing

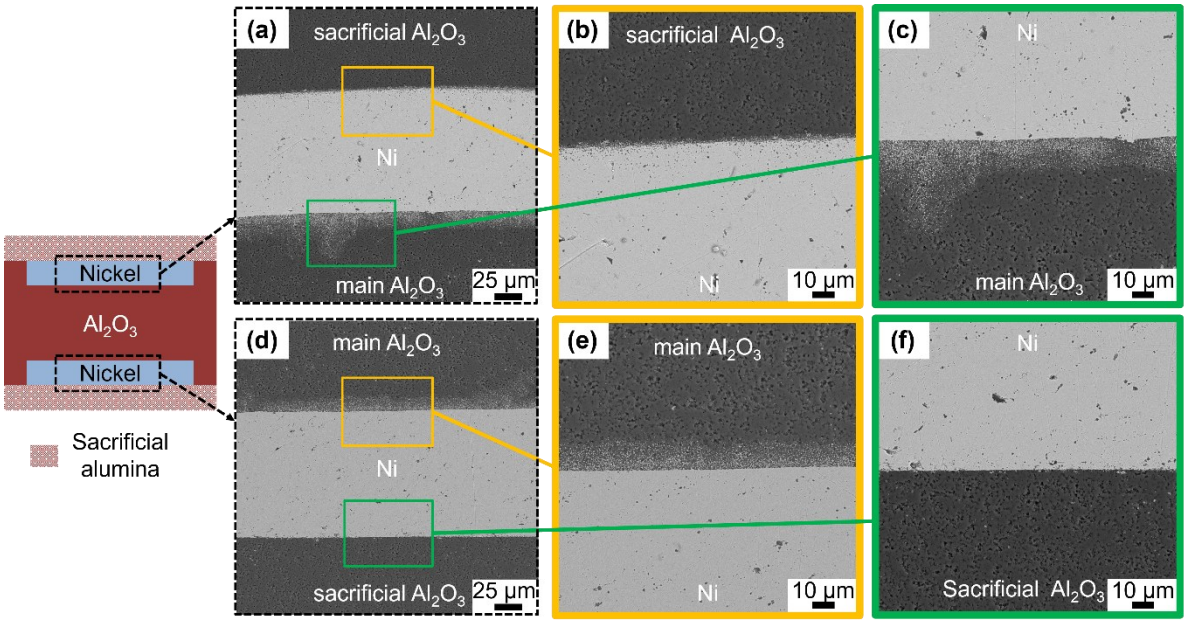

Fig. 7 SEM images of the cross section of the alumina-nickel substrate centered on the Ni foil of the top (a) and bottom (d), an enlargement of the main Al_2O_3 interface (c and e) and sacrificial Al_2O_3 interface (b and f) with Ni

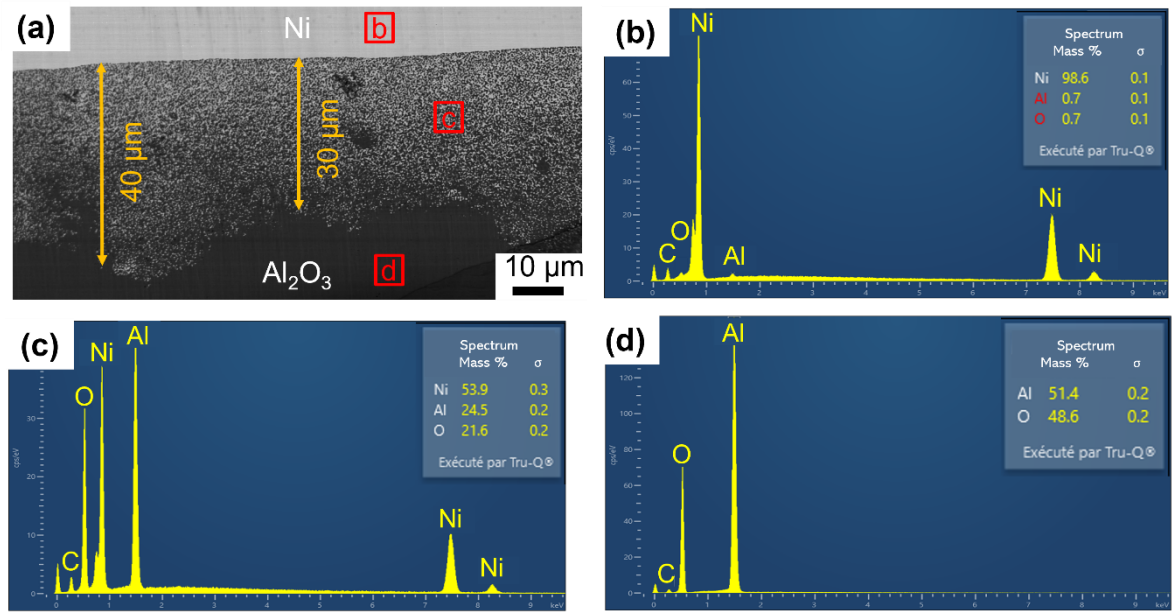

Fig. 8 FEG-SEM image of the Ni/Al_2O_3 interface after cross-polisher cutting (a). EDS spectra of different zones of the interface (b, c and d).

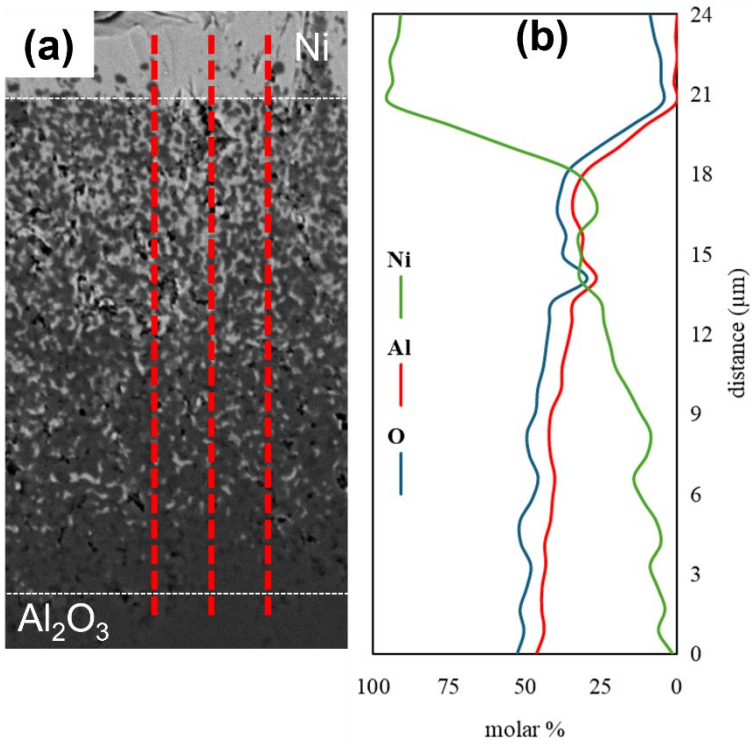

Fig. 9 SEM image of the Ni/Al_2O_3 interface with three-line scan (a) and the average of the corresponding EDS line mapping of Al, Ni and O in molar percentage (b)

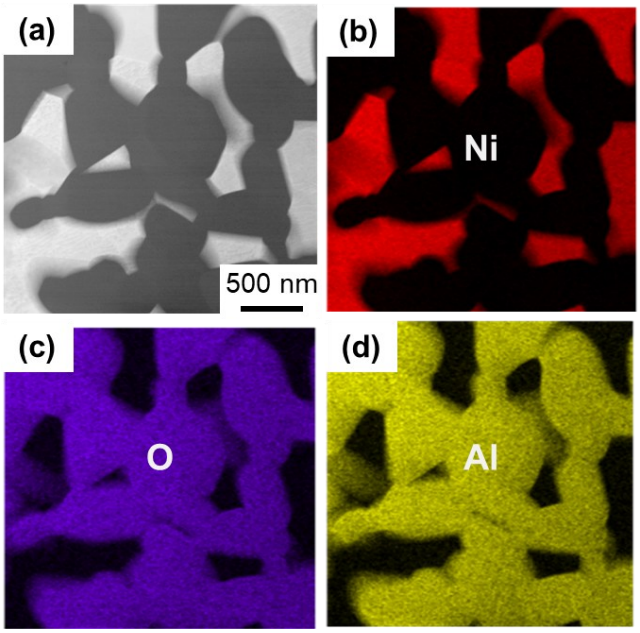

Fig. 10 TEM image of the Ni/Al_2O_3 interface area (a) and EDS analysis of Ni (b), O (c) and Al (d)

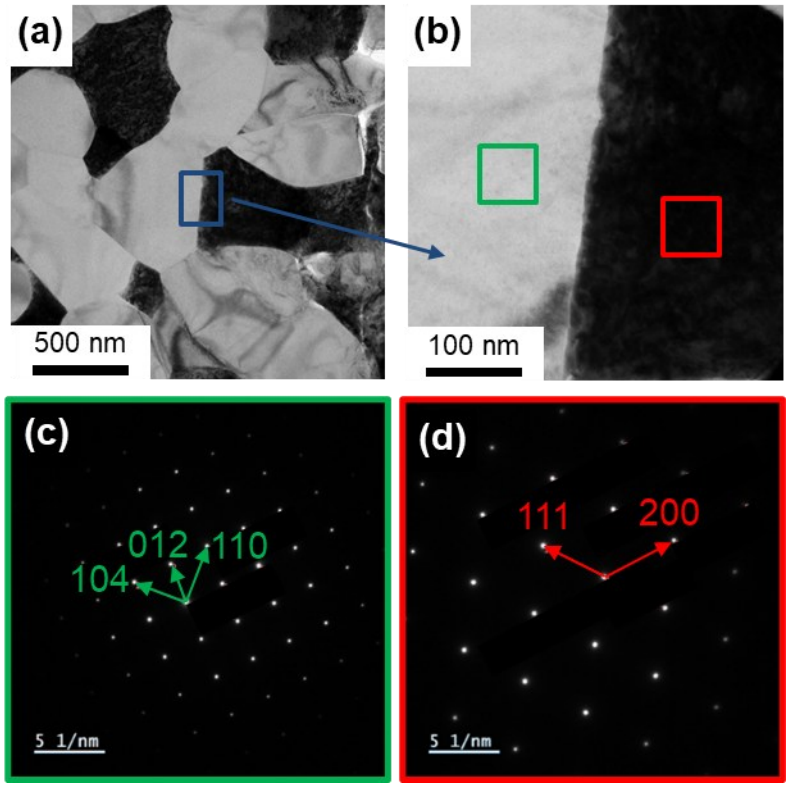

Fig. 11 TEM images of the Ni/Al_2O_3 interface area (a) and an enlargement at the interface of the alumina grain and Ni matrix also the electronic diffraction of these two areas (c and d)

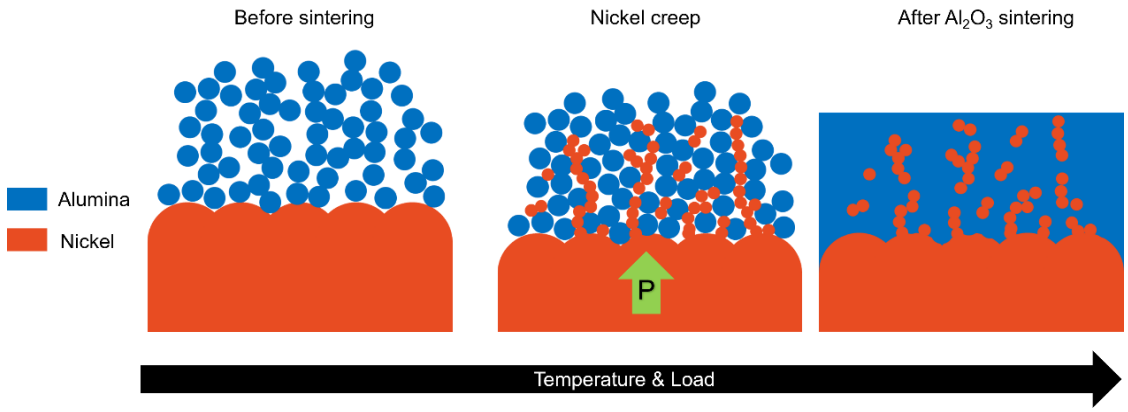

Fig. 12: Schematic representation of the behavior of the Ni/Al_2O_3 interface during the sintering

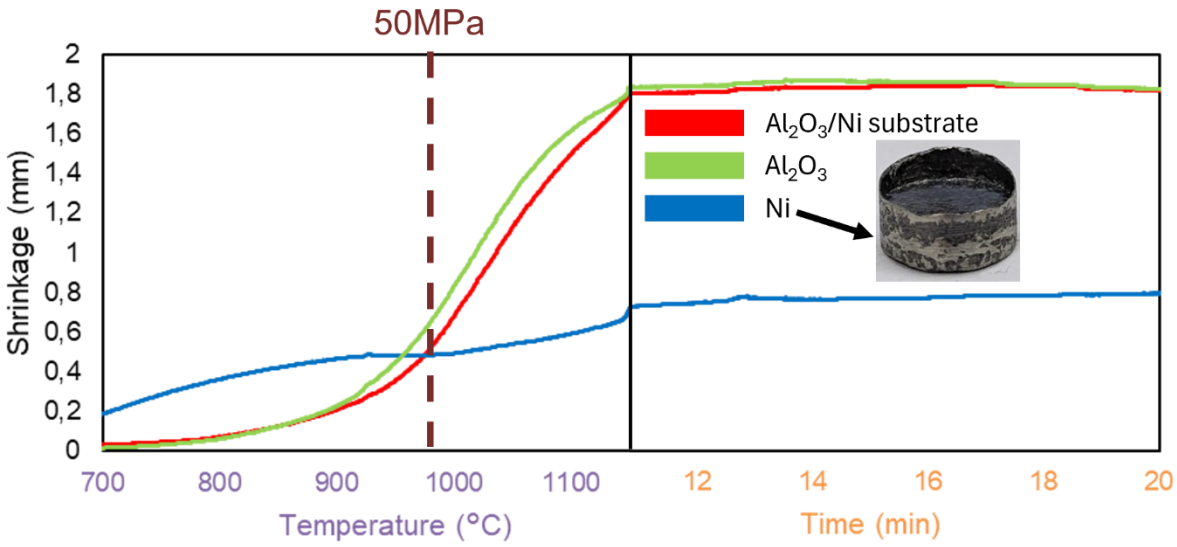

Fig. 13 Shrinkage of the alumina-nickel substrate, alumina and nickel with sacrificial alumina as a function of temperature and time (at 1150°C)